

RESEARCH ARTICLE

Selective Inhibition of Oncogenic KRAS Output with Small Molecules Targeting the Inactive State

Matthew P. Patricelli, Matthew R. Janes, Lian-Sheng Li, Rasmus Hansen, Ulf Peters, Linda V. Kessler, Yuching Chen, Jeff M. Kucharski, Jun Feng, Tess Ely, Jeffrey H. Chen, Sarah J. Firdaus, Anjali Babbar, Pingda Ren, and Yi Liu



ABSTRACT

KRAS gain-of-function mutations occur in approximately 30% of all human cancers. Despite more than 30 years of KRAS-focused research and development efforts, no targeted therapy has been discovered for cancers with KRAS mutations. Here, we describe ARS-853, a selective, covalent inhibitor of KRAS^{G12C} that inhibits mutant KRAS-driven signaling by binding to the GDP-bound oncoprotein and preventing activation. Based on the rates of engagement and inhibition observed for ARS-853, along with a mutant-specific mass spectrometry-based assay for assessing KRAS activation status, we show that the nucleotide state of KRAS^{G12C} is in a state of dynamic flux that can be modulated by upstream signaling factors. These studies provide convincing evidence that the KRAS^{G12C} mutation generates a “hyperexcitable” rather than a “statically active” state and that targeting the inactive, GDP-bound form is a promising approach for generating novel anti-RAS therapeutics.

SIGNIFICANCE: A cell-active, mutant-specific, covalent inhibitor of KRAS^{G12C} is described that targets the GDP-bound, inactive state and prevents subsequent activation. Using this novel compound, we demonstrate that KRAS^{G12C} oncoprotein rapidly cycles bound nucleotide and responds to upstream signaling inputs to maintain a highly active state. *Cancer Discov*; 6(3): 316–29. ©2016 AACR.

See related commentary by Westover et al., p. 233.

INTRODUCTION

Cancer genome sequencing efforts over the past 10 to 15 years have led to the identification of numerous oncogenes responsible for the development and maintenance of human cancers. These discoveries stimulated widespread oncogene-targeted drug-development efforts leading to the approval of a number of novel and efficacious targeted therapies, particularly against targets in the protein kinase family. Notably absent from the growing list of oncogenes with corresponding targeted therapeutics is the first to be discovered, and the most prevalent oncogene in human cancers, RAS. Cancers harboring RAS mutations remain essentially untreatable more than 30 years after the initial discovery of the oncogene.

RAS was for many years considered to be undruggable, but several recent reports have generated renewed interest in the development of direct RAS inhibitors (1). Molecules binding directly to RAS and inhibiting interaction with its activator SOS (2, 3) or effector RAF (4) have been reported. A third published approach specifically and covalently targeted the G12C mutation of KRAS with either electrophilic GDP mimetics (5) or electrophilic compounds targeting a novel allosteric pocket under the Switch II loop region exposed exclusively in the GDP-bound state of KRAS (6). Compounds described in the latter work were found to inhibit RAS activity by blocking SOS-mediated nucleotide exchange and/or

altering the relative affinity of KRAS for GDP versus GTP nucleotide. These innovative approaches demonstrated the presence of previously unknown binding pockets on the surface of RAS and provide a framework for continued efforts to develop novel RAS-targeted therapies.

Importantly, none of the recently presented KRAS-targeting approaches resulted in a compound with clearly demonstrated activity against mutant KRAS in cells. Here, we have focused on the novel Switch II pocket described by Ostrem and colleagues (6) and discovered a compound, ARS-853, with robust cellular activity against KRAS^{G12C} in the low micromolar range. A detailed biochemical and cellular characterization of the mechanism of action of ARS-853 revealed an unexpected plasticity in the nucleotide/activity state of KRAS^{G12C}. As opposed to the classic view of mutant KRAS as a constitutively active enzyme, we have discovered that the KRAS^{G12C} mutant rapidly cycles nucleotide and is thus responsive to upstream signaling inputs. These findings validate an unexpected strategy of targeting inactive mutant KRAS, and further provide a framework for exploring synergistic drug combinations and mechanisms of resistance to mutant KRAS inhibition.

RESULTS**Identification of Inhibitors That Selectively Engage KRAS^{G12C} Oncoprotein in Cells**

In order to further characterize the cellular activity of the previously reported inhibitors and to enable the development of improved KRAS^{G12C} inhibitors with potent cellular activity, we developed an LC/MS-MS-based assay to directly and quantitatively determine engagement of KRAS^{G12C} in a cellular setting (Fig. 1A). Briefly, the decrease of the cysteine 12 (C12)-containing peptide from tryptic digests of KRAS^{G12C}-mutant cells following compound treatment is quantified relative to isotopic standard peptides. Using this assay we found that Compound 12 (6) did not show substantial KRAS^{G12C} covalent engagement in NCI-H358 (H358) cells, which harbor

Wellspring Biosciences, La Jolla, California.

Note: Supplementary data for this article are available at Cancer Discovery Online (<http://cancerdiscovery.aacrjournals.org/>).

M.P. Patricelli and M.R. Janes contributed equally to this article.

Current address for P. Ren and Y. Liu: Kura Oncology, La Jolla, California.

Corresponding Author: Yi Liu, Kura Oncology, 11119 N. Torrey Pines Road, La Jolla, CA 92037. Phone: 858-500-8805; Fax: 858-500-8801; E-mail: yi@kuraoncology.com

doi: 10.1158/2159-8290.CD-15-1105

©2016 American Association for Cancer Research.

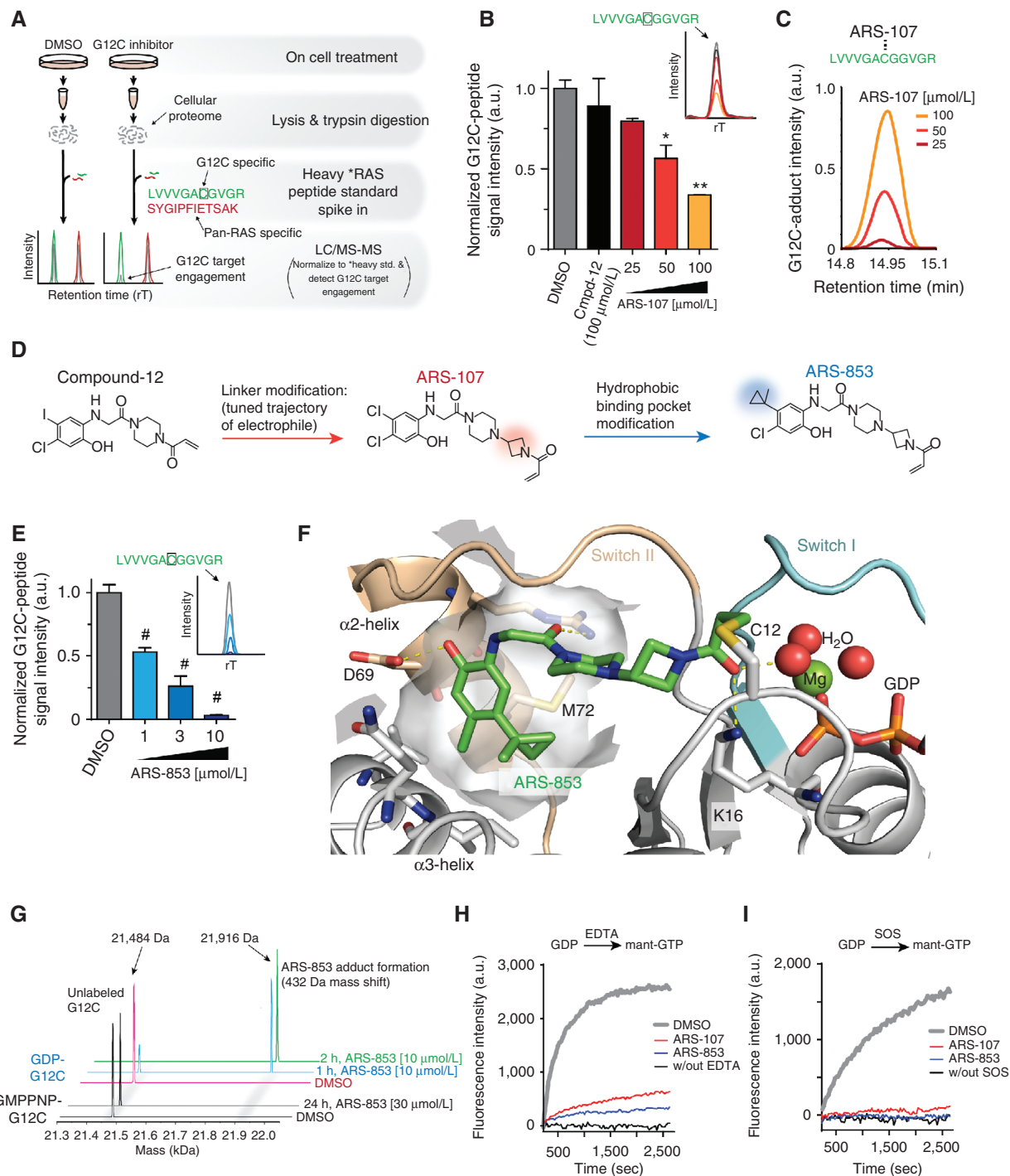


Figure 1. Identification of a covalent KRAS^{G12C} inhibitor active in cells. **A**, schematic of the method for detecting small molecule engagement of KRAS^{G12C} in cells by LC/MS-MS. Engagement is observed as a loss of the C12 containing tryptic peptide (KRAS^{G12C} residues 6-16) relative to a control peptide (KRAS/NRAS residues 136-147). Each peptide is quantified relative to an internal standard (green and red, respectively) spiked in following the tryptic digest. **B**, KRAS^{G12C} signal intensity and LC/MS-MS extracted ion chromatograms of representative runs (upper right) from LC/MS-MS analyses of tryptic digests following 6-hour treatment of H358 cells (*, $P < 0.05$; **, $P < 0.01$). **C**, LC/MS-MS-extracted ion chromatogram showing adduct formation between the KRAS C12 tryptic peptide and ARS-107 in samples from **B**. **D**, chemistry design scheme from Compound 12 to ARS-107 and ARS-853. **E**, KRAS^{G12C} signal intensity and LC/MS-MS analyses of tryptic digests following treatment of H358 cells as indicated for 6 hours (#, $P < 0.001$) (biologic replicates, $n = 3$). **F**, crystal structure of ARS-853 bound to KRAS^{G12C} highlighting key hydrogen bonds and hydrophobic interactions in the Switch II pocket. **G**, deconvoluted electrospray mass spectra of 2 μmol/L KRAS^{G12C} (average MW 21,485) treated with ARS-853 (MW 432) for indicated times. ARS-853 covalently engages GDP-loaded KRAS^{G12C} in a time-dependent manner, but not GMPPNP-loaded active KRAS^{G12C}. **H**, EDTA-mediated nucleotide release assay with GDP-bound KRAS^{G12C} protein prelabeled with the indicated inhibitor, and mant-GTP as excess incoming nucleotide. **I**, SOS-mediated nucleotide exchange assay with GDP-bound KRAS^{G12C} protein prelabeled with the indicated inhibitor, and mant-GTP as incoming nucleotide.

the KRAS^{G12C} mutation, even after a 6-hour treatment with 100 $\mu\text{mol/L}$ compound (Fig. 1B).

To address the possible reasons for the lack of cellular efficacy observed for Compound 12, more potent Switch II pocket inhibitors were needed. With this aim, we performed iterative structure-based design of covalent KRAS^{G12C}-targeted agents and tested candidates for their activity against purified, recombinant KRAS^{G12C}, as well as their ability to engage KRAS^{G12C} in cells. An early strong biochemical hit, ARS-107, exhibited promising KRAS^{G12C} engagement in cells (Fig. 1B). Consistent with the loss of the C12 tryptic peptide of KRAS^{G12C}, we detected a dose-dependent increase in a peptide species matching the adduct of ARS-107 with the C12 tryptic peptide (Fig. 1C). Structural and iterative structure activity relationship (SAR) evaluation of ARS-107 and related compounds suggested that the 5-chloro position on the phenyl ring was critical for activity; thus, this position was the focus of further optimization (Fig. 1D). Several compounds with improved biochemical activity and cellular activity were synthesized (Supplementary Table S1), leading to the most potent compound, ARS-853. ARS-853 engaged KRAS^{G12C} in the biochemical assay with a rate constant of 76 $\text{M}^{-1}\text{s}^{-1}$, a more than 600-fold improvement compared with Compound 12, and a cellular engagement IC_{50} at 6 hours of 1.6 $\mu\text{mol/L}$ (Fig. 1E; Supplementary Table S1).

The high-resolution crystal structure of ligand-bound KRAS^{G12C} in the presence of GDP confirmed the binding site of ARS-853 as the previously described Switch II pocket (Fig. 1F; Supplementary Fig. S1A–F; Supplementary Table S2). In the structure, ARS-853 is covalently attached to C12 and extends into the Switch II pocket region located between the central beta-sheet of KRAS and the $\alpha 2$ and $\alpha 3$ helices. Relative to other published structures of Switch II-bound compounds, ARS-853 induces a rotation of the $\alpha 2$ helix accompanied by a shift of M72 to accommodate the ligand in a distinct hydrophobic pocket. This hydrophobic pocket is occupied by the aromatic ring of ARS-853 with the chloro- and methylcyclopropyl substituents providing tight van der Waals contacts, while the phenolic hydroxyl group makes a hydrogen bond with D69. The carbonyl group of the acrylamide warhead of ARS-853 makes hydrogen bonds to the conserved K16 and to one of the water molecules coordinated to the customary magnesium ion while occupying a position similar to the terminal phosphate in the GTP-bound form of KRAS. In the bound structure, both Switch I and Switch II adopt ordered conformations distinct from their active forms, suggesting that binding to activator or effector proteins may be impaired. Overall, multiple features of the structure suggest that ARS-853-bound KRAS^{G12C} represents an inactive state of KRAS.

The structural evaluation of ARS-853 suggested several promising possible mechanisms for inhibition of KRAS function, including interference with GTP binding, stabilization of bound $\text{Mg}^{2+}/\text{GDP}$, and/or blocking activator and/or effector binding in the Switch II region. These possibilities were directly explored in biochemical assays. Although ARS-853 reacted rapidly and selectively with GDP-bound KRAS^{G12C}, we were unable to detect reaction of ARS-853 with GTP-bound KRAS^{G12C} (Fig. 1G; Supplementary Table S3). This strong preference for reaction with GDP-bound KRAS^{G12C} is consistent with the positioning of C12-bound acrylamide carbonyl oxygen in the space typically occupied by the GTP γ -phosphate. Evaluation

of the nucleotide exchange properties of KRAS^{G12C} bound to ARS-853 further confirmed the structural predictions. Following reaction with ARS-853, GDP-bound KRAS^{G12C} showed a dramatic decrease in EDTA catalyzed nucleotide release in the presence of either GTP or GDP as excess incoming nucleotides (Fig. 1H; Supplementary Fig. S2A–D). The extent of this bound Mg^{2+} -GDP stabilization effect correlated with compound engagement potency across a set of ARS-853-related compounds (Fig. 1H; Supplementary Fig. S2A–D), suggesting cooperative binding between the Mg^{2+} -GDP and the covalent inhibitor. This effect may be correlated structurally with the indirect Mg^{2+} coordination observed in the crystal structure. ARS-853 and related analogues completely inhibited SOS catalyzed nucleotide exchange with either GDP or GTP as incoming nucleotide (Fig. 1I; Supplementary Fig. S2E–H), consistent with both Mg^{2+} stabilization and general interference with Switch II function. Together, these data suggest an inhibitory mechanism of action whereby ARS-853 reacts specifically with GDP-bound KRAS^{G12C}, and once bound prevents formation of the GTP-bound state through either intrinsic or catalyzed exchange mechanisms.

Before evaluating the effects of ARS-853 on cell functional readouts, we directly assessed its covalent selectivity across free cysteines in the proteome using an assay similar to that described by Wang and colleagues (ref. 7; Fig. 2A–B; Supplementary Fig. S3; Supplementary Table S4). Across the 2,740 surface-exposed cysteine residues profiled from 1,584 proteins, KRAS^{G12C} was the most potently engaged target observed. Only two other targets, FAM213A and Reticulon-4 (RTN4), displayed significant engagement at doses lower than 30 $\mu\text{mol/L}$. Importantly, these two off-targets were also observed in A549 cells, which harbor the G12S oncogene and were chosen as a control line for subsequent studies (Fig. 2C).

ARS-853 Inhibits KRAS^{G12C} Oncoprotein Function in Cells

We investigated the cellular effects of ARS-853 by monitoring the impact of treatment on active KRAS levels and RAS-mediated signaling in cells. ARS-853 treatment of KRAS^{G12C} cells led to a dose-dependent and nearly complete inhibition of CRAF-RBD (RBD)-mediated pulldown of KRAS from lysates, with an IC_{50} of approximately 1 $\mu\text{mol/L}$ (Fig. 3A, left). The effect of ARS-853 treatment on the critical interaction of active KRAS with its effector protein CRAF in cells was determined by a proximity ligation assay (Fig. 3B). This method allows for the visualization of cellular KRAS–CRAF interactions through the proximity-dependent annealing and amplification of homologous DNA sequences present on antibodies to the two respective targets. Treatment of H358 cells by ARS-853 resulted in a significant loss of KRAS–CRAF interactions. Consistent with an inactive state of KRAS^{G12C} once bound to ARS-853, downstream signaling through both MAPK (including pMEK, pERK, and pRSK) and PI3K signaling (pAKT) pathways was inhibited by ARS-853 in H358 and other KRAS^{G12C} cell lines (Fig. 3A; Supplementary Fig. S4A–C). The inhibition of RAF-RBD pulldown and KRAS downstream signaling was sustained over a period of 72 hours (Fig. 3C), accompanied by G₁ cell-cycle arrest (Supplementary Fig. S4B), loss of Cyclin D1 and Rb expression, and an increase in the cell-cycle inhibitor p27 KIP1 (Fig. 3C; Supplementary Fig. S4A). In addition,

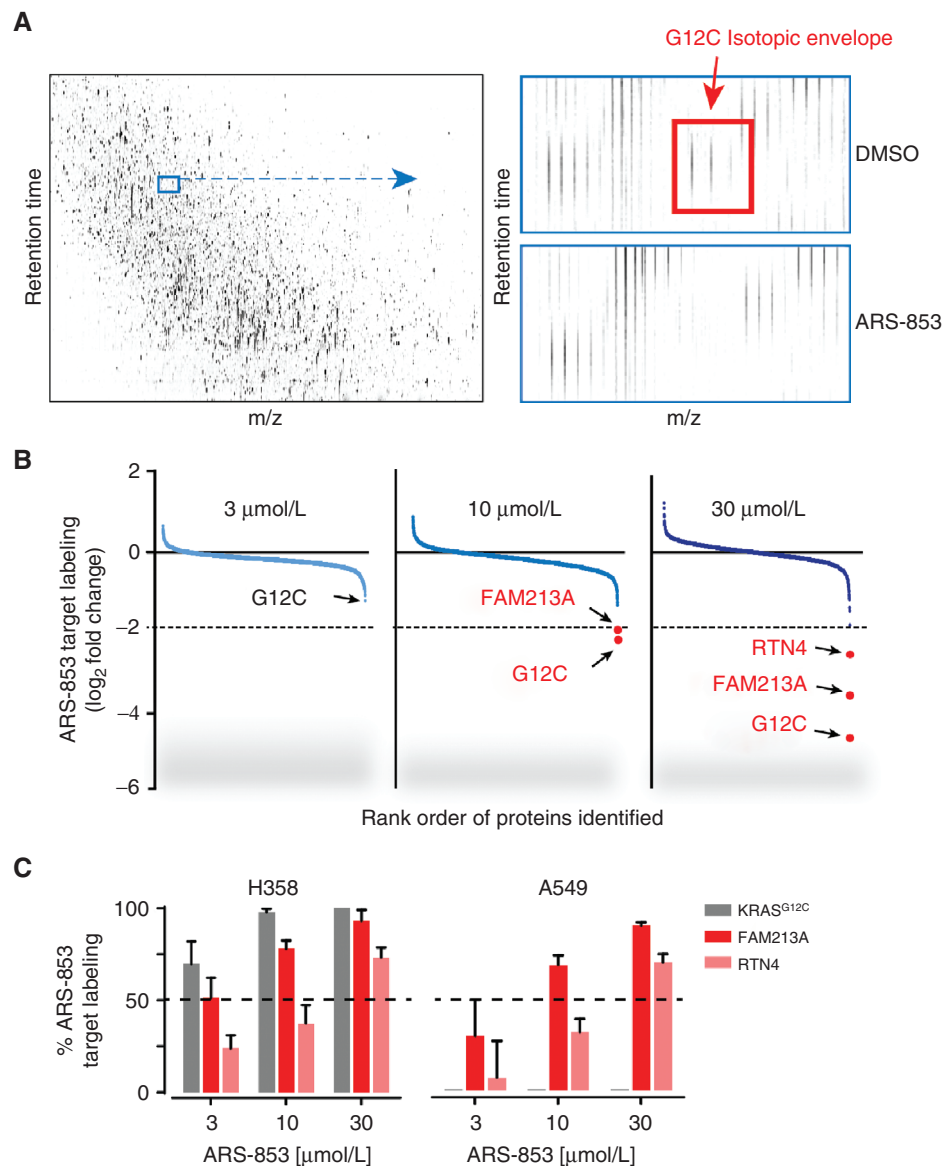


Figure 2. Proteomic cysteine profiling of ARS-853 selectivity. **A**, mass to charge ratio (m/z) versus retention time plot of MS analysis of samples treated as described in methods for proteomic cysteine profiling (left) and a magnified comparison of the region containing the $KRAS^{G12C}$ tryptic peptide following treatment with ARS-853 (right) for 4 hours. **B**, rank ordering by fold change of ARS-853-targeted proteins identified by MS-based proteomic cysteine profiling. Targets showing more than 4-fold decrease are annotated in red. **C**, targeted cysteine selectivity profiling comparing the labeling of $KRAS^{G12C}$, FAM213A, and RTN4 following treatment with ARS-853 for 4 hours.

hallmarks of apoptosis, including cleaved PARP (Fig. 3A) and increases in sub-diploid DNA (Supplementary Fig. S4B), were observed in H358 cells following treatment with ARS-853. We observed no effects on RAF-RBD binding or downstream signaling in A549 cells ($KRAS^{G12S}$, Fig. 3A, right), and the inhibitory effects of ARS-853 in H358 cells could be rescued by ectopic expression of $KRAS^{G12V}$ (Fig. 3D), highlighting the selectivity of ARS-853 for the $KRAS^{G12C}$ oncoprotein.

Consistent with its specific and complete ability to inhibit $KRAS^{G12C}$ signaling, ARS-853 selectively inhibited the growth of H358 cells in culture (Fig. 4A–D). Growth inhibition in H358 cells could be rescued by ectopic expression of $KRAS^{G12V}$ (Fig. 4A), and was observed for $KRAS^{G12C}$, but not for

$KRAS^{G12V}$ oncogenic transformation of NIH-3T3 fibroblasts (Supplementary Fig. S5) supporting the $KRAS^{G12C}$ oncoprotein-specific activity of ARS-853. In further support of an on-target mechanism of action, a small series of active and inactive structural analogues of ARS-853 inhibited the two-dimensional/adherent (2-D) proliferation of $KRAS^{G12C}$ -bearing H358 cells with a potency trend strongly correlating with biochemical and cellular target engagement (Supplementary Fig. S6; Supplementary Table S1).

Across a panel of cell lines, ARS-853 inhibited proliferation in 2-D growth assays in only a subset of the $KRAS^{G12C}$ lines tested (Fig. 4B, left). Despite the lack of growth inhibition in some lines, we found that ARS-853 effectively inhibited RAF-RBD

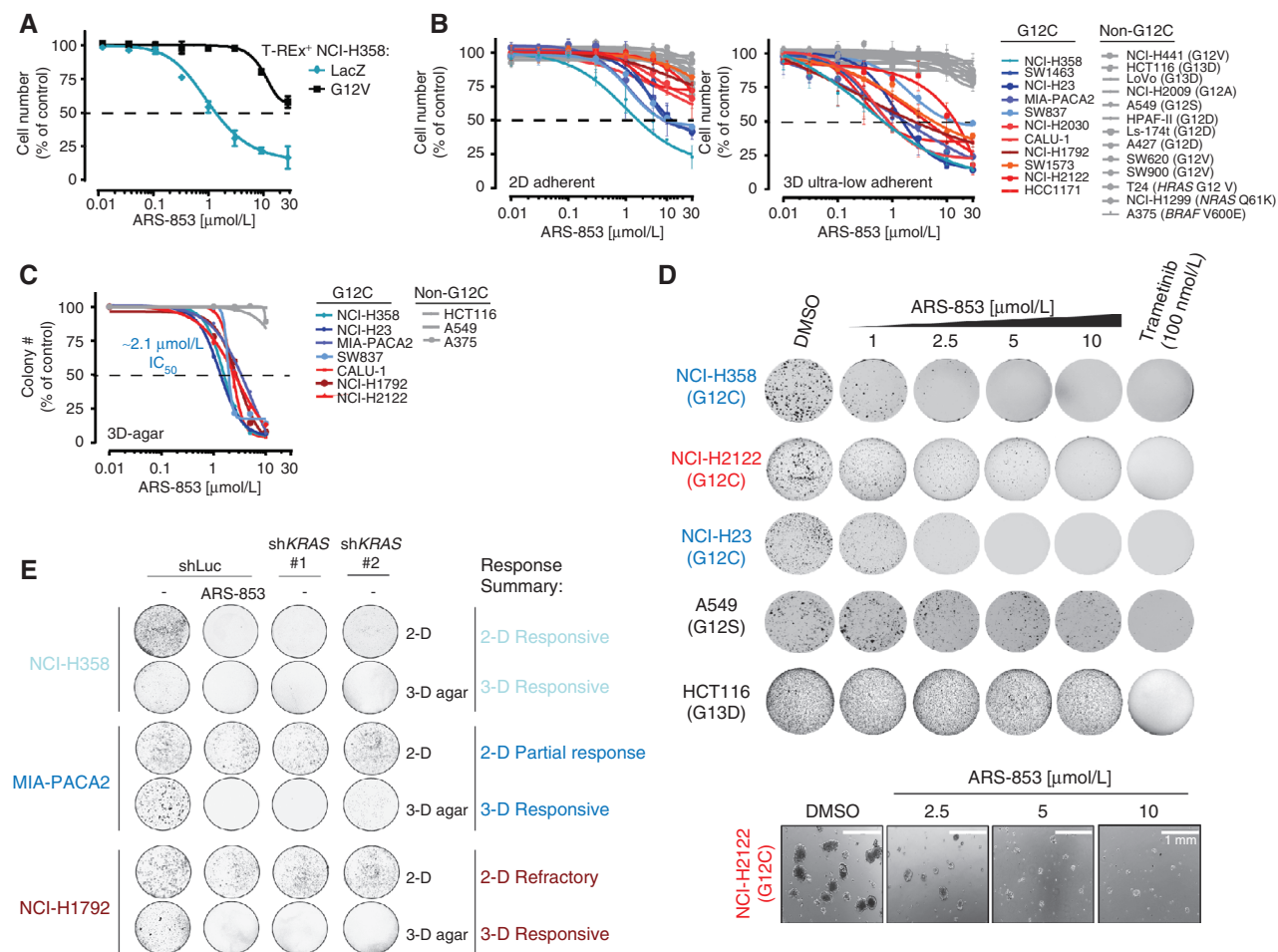


Figure 4. Cellular activity and selectivity of ARS-853. **A**, T-REx H358 cells stably expressing LacZ/TO or FLAG-KRAS^{G12V}/TO were cultured with doxycycline (10 ng/mL) 24 hours prior to treatment with indicated amounts of ARS-853. Effects on cell growth were monitored 5 days later by CellTiter-Glo. **B**, the effects on adherent cell growth (left) or 3-D ultra-low adherent cell growth (right) following 5-day treatment with ARS-853. **C**, the effects on anchorage-independent growth in soft agar following 14-day treatment with ARS-853. Error bars, mean \pm SD [across at least 2 independent experiments (**B**) or biologic duplicate wells (**C**), respectively]. **D**, representative images of crystal violet-stained colony formation in soft agar displayed from **C** (top) and magnified representative images of NCI-H2122 following 10 days of treatment (bottom). **E**, the effects of KRAS knockdown or ARS-853 treatment on growth in 2-D adherent or in 3-D soft-agar formats. Cells (20,000) stably transduced with lentivirus expressing shLuc or shKRAS were plated 48 hours following transduction in media containing 1 $\mu\text{g/mL}$ puromycin in either 2-D adherent or 3-D soft-agar formats. Twenty-four hours following plating, cells were treated with or without ARS-853 (10 $\mu\text{mol/L}$). Growth was monitored after 10 to 14 days, and representative images of crystal violet-stained colony formation are depicted (see also Supplementary Fig. S7).

surprising given the expectation that mutant KRAS would be locked in a fully active state. ARS-853 showed exquisite selectivity for the GDP-bound form of KRAS^{G12C} (Fig. 1G; Supplementary Table S3) which would likely exist at low levels in cells, yet the compound was clearly capable of achieving near-complete engagement and functional inhibition of cellular KRAS^{G12C}. To further investigate this surprising finding, we performed a series of studies to explore KRAS^{G12C} nucleotide cycling properties using ARS-853 as a “GDP-state titrant.” An acute time and dose-response analysis of cell engagement in H358 cells demonstrated that high doses of ARS-853 (>10 $\mu\text{mol/L}$) achieved engagement levels >90% within 2 hours (Fig. 5A). At these high doses, the engagement rate showed an initial burst (at 15 minutes) to an apparent rate-saturated level of ~45% engagement, followed by a slower rate of continued engagement that reached well over 90% by 2 hours. Time and

dose dependence of the inhibition of active KRAS, and downstream signaling markers were consistent with the KRAS^{G12C} engagement data (Fig. 5B).

The cellular engagement kinetics for ARS-853 did not fit a typical/expected pseudo-first order curve, indicating the possibility that factors such as resting GDP-KRAS^{G12C} levels, and nucleotide cycling rates may be affecting engagement rates. Importantly, engagement of the off-target RTN4 protein (monitored simultaneously in the assay) showed a normal dose and time response at the high concentrations where KRAS engagement rates were saturated (Supplementary Fig. S8). To assess the rates of the underlying nucleotide cycling of KRAS, we fit the engagement dose/time-response data using a kinetic model including variable parameters for nucleotide exchange, GTP hydrolysis, and ARS-853 engagement rate (Fig. 5A). The model provided

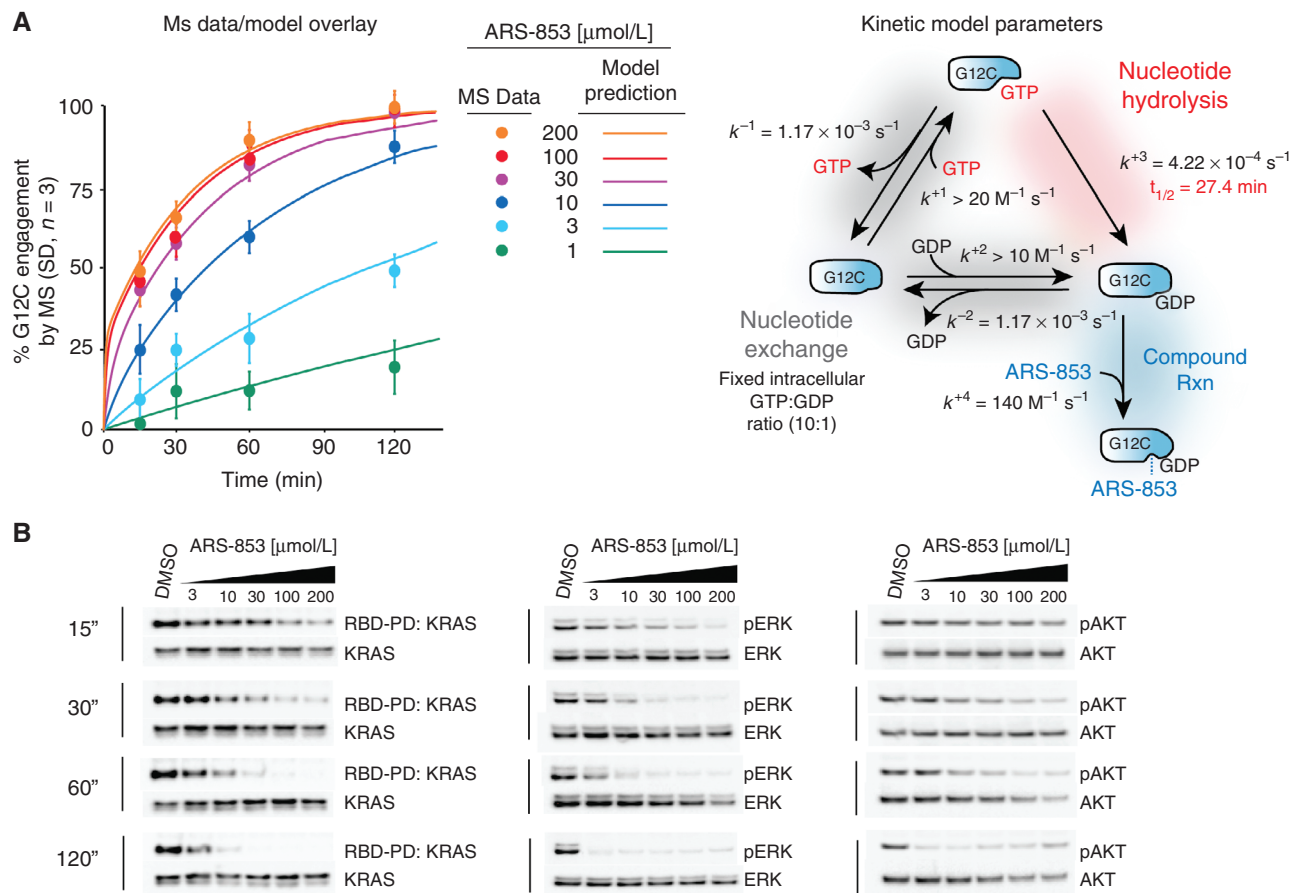


Figure 5. The kinetics of cellular G12C engagement and signaling inhibition with a GDP-state selective inhibitor demonstrates rapid nucleotide cycling of KRAS^{G12C} between GTP- and GDP-bound states. **A**, LC/MS-MS analysis of KRAS^{G12C} engagement following treatment of H358 cells (circles) overlaid with a fit (lines) based on nonlinear regression to a kinetic model depicted on the right. The kinetic model (right) incorporates parameters for KRAS^{G12C} nucleotide cycling with ARS-853 cellular engagement with best-fit values to the experimental data. **B**, immunoblots showing kinetics and dose response of ARS-853 on KRAS-GTP by RBD pulldown (RBD-PD), and the effects on downstream RAS signaling activation markers for MAPK (pERK T202/Y204), and PI3K/mTOR (pAKT S473).

a good fit to the data, with half-lives for nucleotide release and hydrolysis of ~ 9.9 and 27 minutes respectively and a rate constant for ARS-853 engagement with GDP-KRAS of $140 \text{ M}^{-1} \text{ s}^{-1}$. The value determined for KRAS^{G12C} nucleotide exchange rate in cells is significantly faster than the intrinsic exchange rates determined by us (Supplementary Table S5) and others (13, 14). A recent comparison of KRAS position 12 mutant properties, however, found that KRAS^{G12C} hydrolyzed GTP with a half-life of 23 minutes (14), significantly faster than other mutants and consistent with our cellular characterization.

KRAS^{G12C} GTP Levels Are Modulated by Upstream Signaling Factors

The faster-than-expected nucleotide cycling of KRAS^{G12C} in cells prompted us to explore the intriguing possibility that mutant KRAS-GTP levels are regulated by the same signaling mechanisms that regulate wild-type (WT) RAS isoforms, such as growth factor receptor activation (Fig. 6A). Because H358 cells are heterozygous for KRAS^{G12C}, we needed an assay capable of distinguishing the activation status of the KRAS^{G12C}

oncoprotein from the WT-KRAS isoform. To achieve this goal, we developed a mass spectrometry-based approach using the RAF-RBD as in the traditional active RAS pulldown assay, but incorporating a GMPPNP-bound, stable isotope-modified KRAS^{G12C} (heavy KRAS^{G12C}) protein as an internal reference. The heavy KRAS^{G12C} standard is added to lysates immediately prior to the RAF-RBD capture step, and a quantitative LC/MS-MS analysis focused on the residue 12 containing tryptic peptide (to differentiate WT and G12C isoforms) is used to determine the active fraction of endogenous (light) KRAS^{G12C} relative to the standard (RBD-MS assay; Supplementary Fig. S9A). By adding a GMPPNP-loaded heavy NRAS standard, we are also able to quantify the active fraction of the combined WT-RAS pool (Supplementary Fig. S9B). Following treatment with the EGFR inhibitor erlotinib, we observed a significant, time-dependent decrease in the KRAS^{G12C} GTP fraction (Fig. 6B and C; Supplementary Fig. S10). Using the general kinetic model for KRAS nucleotide cycling described above (Fig. 5A), the best fit of the erlotinib-induced loss of active KRAS suggested a GTP hydrolysis half-life of 27 minutes, consistent with the kinetic modeling of ARS-853 engagement. Following

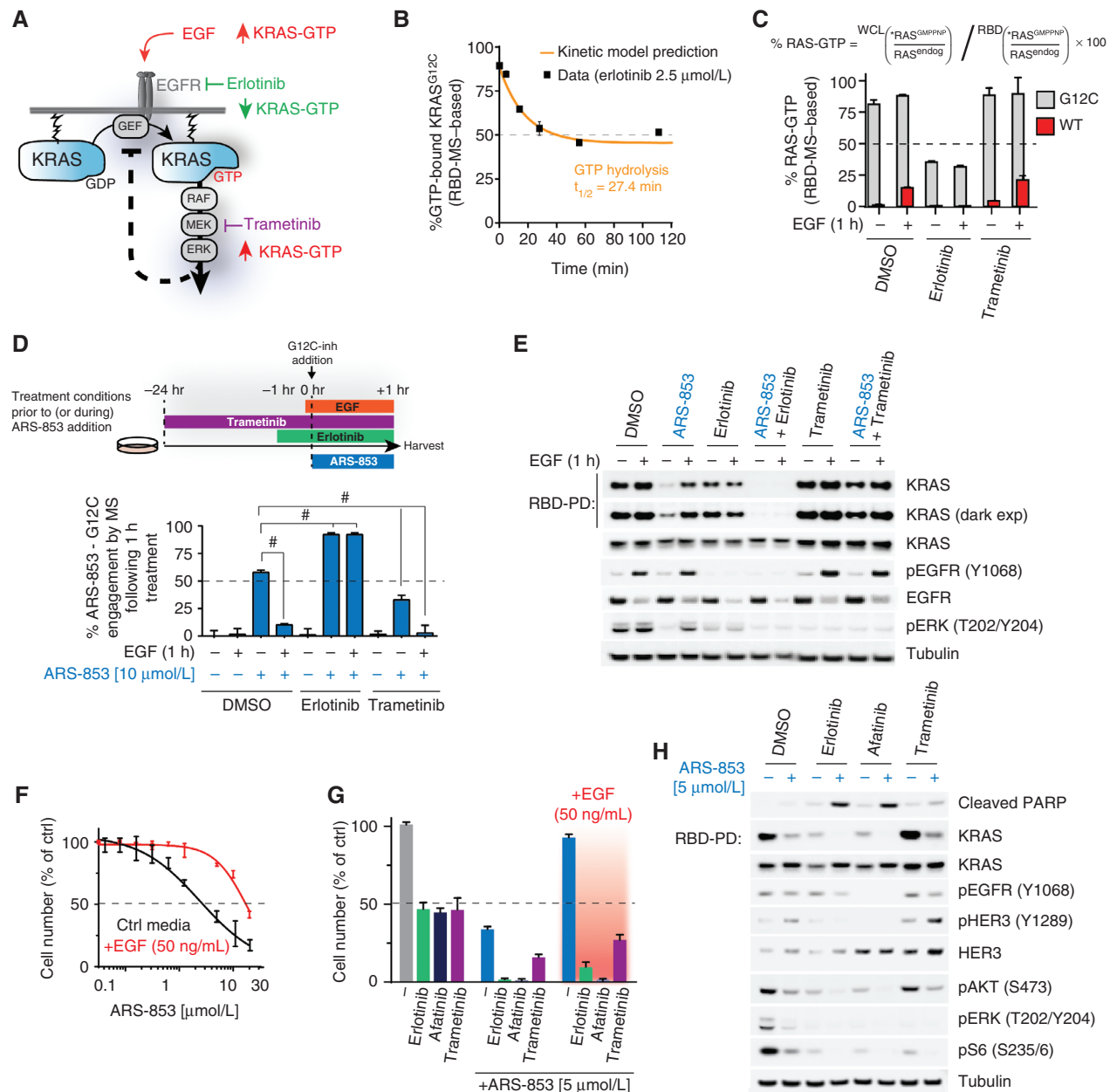


Figure 6. Modulation of KRAS^{G12C} activity alters ARS-853 target engagement and supports novel therapeutic strategies for targeting KRAS. **A**, schematic for altering KRAS-GTP through growth factor or small molecule inhibitors. **B**, RBD-MS analysis of H358 cells treated with erlotinib (2.5 μmol/L) harvested at the indicated time points. Experimental data values were used as input into the kinetic model parameters shown in Figure 4A (right). The fit estimates a GTP hydrolysis rate half-life on KRAS^{G12C} of 27 minutes. **C**, RBD-MS analysis of GTP-bound KRAS^{G12C} and WT-RAS (K/N/H isoforms) following pretreatment of H358 cells with EGF (100 ng/mL, 1 h), erlotinib (2.5 μmol/L, 2 hours), or trametinib (100 nmol/L, 24 hours). Top, the formula used for calculating %RAS-GTP by the RBD-MS assay (see also Supplementary Fig. S6 for details). **D**, LC/MS-MS-based detection of KRAS^{G12C} target engagement by ARS-853 (10 μmol/L, 1 h) in H358 cells treated with the indicated agent to alter the RAS-GTP fraction. Top, timing and design of pretreatment or cotreated conditions: trametinib (100 nmol/L) was added 24 hours prior, and erlotinib (2.5 μmol/L) 1 h prior to ARS-853 addition, and EGF (100 ng/ml) was cotreated with ARS-853. #, *P* < 0.001 by ANOVA compared with ARS-853 treatment alone. ARS-853 cell engagement is modulated consistent with specific reactivity to GDP-bound KRAS^{G12C}. **E**, immunoblot experiment from biologic replicate lysates depicted in **D**. **F**, antiproliferative effects of ARS-853 treatment of H358 cells cultured with or without EGF (50 ng/mL) for 5 days. **G**, antiproliferative effects of combination treatments (0.4 μmol/L erlotinib, 0.1 μmol/L afatinib, or 50 nmol/L trametinib), on H358 cells cultured with or without EGF (50 ng/mL) for 5 days. **H**, immunoblot assessment KRAS signaling following 24 hours treatment of H358 cells with ARS-853 in combination with erlotinib (5 μmol/L), afatinib (100 nmol/L), or trametinib (100 nmol/L).

erlotinib treatment, we treated cells with ARS-853 and observed a significant increase in KRAS^{G12C} engagement, consistent with an increase in the compound accessible GDP-bound KRAS^{G12C} fraction (Fig. 6D). In contrast, when H358 cells were treated with EGF (50 ng/mL) to increase upstream

signaling input to RAS, the active KRAS^{G12C} fraction increased from 81% to 88%–91% (which would correspond to a ~2-fold decrease in the level of GDP-bound KRAS^{G12C}), and ARS-853 engagement was significantly reduced (Fig. 6C and D). Furthermore, 24-hour pretreatment with trametinib, to induce

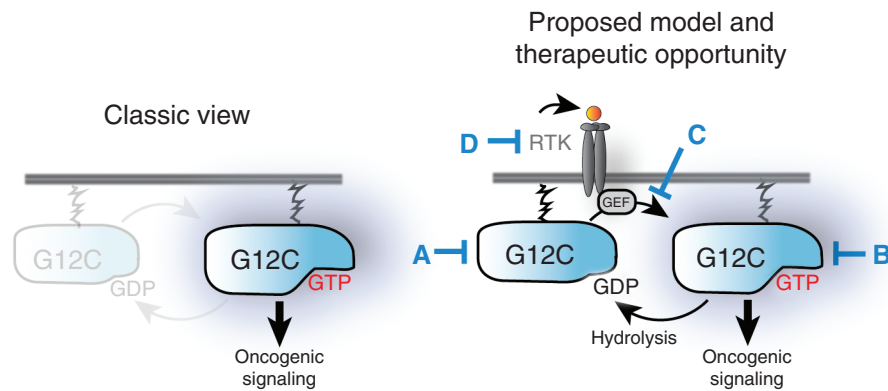


Figure 7. Schematic models of the conventional (left) and proposed model (right) for the maintenance and modulation of active mutant KRAS levels. The proposed model presents mutant KRAS^{G12C} in a rapidly cycling state, whereby nucleotide exchange and hydrolysis occur and require signaling inputs (likely through exchange factors) to maintain high levels of the active, GTP-bound state. This model supports the following therapeutic opportunities as single agents or combinations: A, targeting the inactive-GDP bound state; B, targeting the active, GTP-bound state (an area of assumed focus as sole strategy); and C, targeting the RAS Guanine nucleotide exchange factor (GEF), or (D) alternative upstream inputs that regulate RAS-GEFs.

relief of negative feedback to RAS (15–17), increased HER3 activation (18, 19) and active KRAS^{G12C} levels while concomitantly reducing engagement (Fig. 6C and D). The effects of the inhibitor and growth factor-induced modulation of both KRAS-GTP levels and ARS-853 engagement were also observed in downstream signaling assays (Fig. 6E). Levels of active, GTP-bound WT-KRAS were increased, as expected by both EGF and trametinib treatments, but remained significantly lower than the mutant with all treatments (Fig. 6C). These results demonstrate that the activity of KRAS^{G12C} is not dictated only by intrinsic properties of the mutant protein, but rather can be modulated by signaling factors in a manner similar to WT-RAS isoforms, albeit with much higher active (GTP) fractions than WT-RAS isoforms.

We next tested the implications of the observed maintenance and regulation of KRAS^{G12C} nucleotide cycling on ARS-853 potency and efficacy in the setting of growth factor and drug combinations. When H358 cells were cultured in the presence of added EGF (50 ng/mL), the ARS-853 inhibition curve was right-shifted roughly 10-fold (Fig. 6F and G). Coadministration of erlotinib or afatinib with ARS-853 greatly potentiated growth arrest over single-agent ARS-853 treatment, even in the presence of added EGF (Fig. 6G; Supplementary Fig. S11A–C). In addition, combinations of ARS-853 with EGFR inhibitors more completely inhibited KRAS pulldown in the RBD assay, and downstream PI3K and MAPK signaling, accompanied by dramatic induction of apoptosis (Fig. 6H; Supplementary Fig. S11). The fact that complete inhibition of PI3K signaling can be achieved only by combined RTK and KRAS inhibition, leading to high levels of apoptosis, is consistent with published reports (20). Interestingly, we observed that the combination of trametinib with ARS-853 was less favorable based on its limited impact on growth arrest, RBD pull-down inhibition, PI3K pathway signaling, and apoptosis induction relative to ARS-853 alone. This may be due to counteracting effects of trametinib of reducing ARS-853 engagement and inhibiting MAPK signaling inhibition (Fig. 6G and H). These results highlight the implications of KRAS^{G12C} nucleotide cycling for inhibitors, like ARS-853,

that target GDP-bound mutant KRAS. Although high levels of growth factor signaling may significantly reduce single-agent efficacy by such an approach, combinations with appropriate agents to mitigate upstream KRAS activation pressure can overcome this mechanism of resistance and provide significant benefit over a single-agent KRAS^{G12C} inhibitor (Fig. 7).

DISCUSSION

ARS-853 is the first direct KRAS inhibitor shown to selectively inhibit KRAS in cells with potency in the range of a drug candidate. Previously reported KRAS inhibitors have either shown insufficient potency for detailed cellular characterization (2, 3, 6), or exhibit dramatic deviations in potency across assays (4). The most potent covalent KRAS^{G12C} ligand reported previously (Compound 12) exhibited promising *in vitro* properties, but its cellular effects were less clear (6). Here, we demonstrate that Compound 12 is not capable of engaging KRAS^{G12C} in cells even at a relatively high dose and long incubation (100 μ mol/L for 6 hours). However, by improving upon the groundbreaking approach of targeting the Switch II pocket of KRAS^{G12C} with covalent ligands, we have successfully identified a covalent inhibitor that demonstrates consistent low micromolar activity from biochemical and cellular engagement to KRAS^{G12C} activation, downstream signaling, and cell survival. Further, we have found that KRAS^{G12C} is the most potent covalent target of ARS-853 across more than 2,700 cellular proteins and consistently find that this compound exerts no effects on cellular signaling or growth in non-KRAS^{G12C} cells at concentrations up to 10-fold higher than its KRAS^{G12C} potency. These studies clearly establish that ARS-853 is a selective and highly efficacious KRAS^{G12C} inhibitor with low micromolar potency in cells.

Similar to the previously characterized Switch II pocket KRAS^{G12C} inhibitor, ARS-853 reacts only with the inactive (GDP-bound), but not the active (GTP-bound), state of KRAS. Mutant RAS proteins have been shown to exist predominantly in the GTP-bound state (21–24) and the overall “cycle time” (change of nucleotide due to either exchange or hydrolysis) of

G12D and G12V mutant KRAS were reported to be >3 hours (21). These properties would seem to preclude substantial cellular engagement, and/or decrease of mutant KRAS-GTP levels through targeting of the GDP-bound form of KRAS^{G12C} (Fig. 7, left). The cellular studies presented here demonstrate that ARS-853 is capable of achieving high levels of engagement and inducing dramatic reductions in active KRAS^{G12C} levels and downstream signaling, despite targeting only GDP-bound KRAS^{G12C}. The combination of our studies using ARS-853 as a tool compound to quantitatively interrogate the GDP-bound state of KRAS, and our novel RBD-MS approach to quantitatively and specifically measure mutant KRAS-GTP levels, demonstrate that KRAS^{G12C} is not locked in a fully activated state, but rather rapidly cycles its nucleotide state, allowing ARS-853 to achieve complete binding/inhibition over time as the oncoprotein cycles its bound nucleotide (Fig. 7, right).

Based on the structural and biochemical effects of ARS-853, particularly the dramatic stabilization of bound GDP preventing intrinsic and/or forced (EDTA) exchange and a complete block of enzymatic (SOS) exchange, we favor a mechanism of inhibition whereby KRAS^{G12C} is unable to achieve the GTP-bound state once bound by ARS-853. Although this precise mechanism is difficult to prove directly in cells, our cellular signaling and proliferation studies clearly demonstrate that ARS-853 binding to KRAS^{G12C} leads to a generally inactive state of the oncoprotein. ARS-853 is therefore a valuable pharmacologic tool to study KRAS function in cells that both complements and provides significant advantages over previously explored transcript and gene-targeted approaches (11, 12, 25). Perhaps most importantly, the rapid inhibition of mutant KRAS signaling by ARS-853 will enable the interrogation of the connectivity and responsiveness of mutant KRAS signals prior to the induction or relief of compensating feedback mechanisms (19, 25). This will be invaluable for understanding the mechanisms underlying the reported variability of KRAS dependence across cell lines observed by us and others (8–10). From our initial studies of KRAS^{G12C}-mediated signaling across cell lines (Supplementary Fig S4A) we have observed varying degrees of ARS-853 inhibition of downstream MAPK/PI3K signaling across the group of cell lines tested, suggesting that there are possible KRAS-independent mechanisms for maintenance of RAS signaling and that these inputs may contribute to differences in mutant KRAS dependence. Our studies with ARS-853 presented here have additionally confirmed that KRAS dependence is much more profound and universal in anchorage-independent settings. Future studies exploring the effects of KRAS^{G12C} inhibition on signaling in adherent and anchorage-independent settings may lead to a better mechanistic understanding of this feature of KRAS biology.

The observation that KRAS^{G12C} activity levels are responsive to growth factor stimulation and inhibition supports further exploration of approaches targeting potential upstream KRAS inputs. The interaction of KRAS with its activator SOS (2, 3, 26–28), for example, may be a valid approach to suppress KRAS oncogenic signaling, at least in the setting of KRAS^{G12C}-mutant tumors. Additionally, combination regimens of KRAS^{G12C}-targeted agents with inhibitors of targets upstream of KRAS may specifically enhance efficacy in KRAS^{G12C}-harboring tumors. Importantly, although we have shown here that EGFR signaling can support active KRAS^{G12C} levels, it is likely that the

specific signaling inputs to KRAS will be cell type-specific. Thus, choosing the most effective combination agent may require an understanding of tumor-specific signaling vulnerabilities upstream of KRAS. Finally, the finding that KRAS^{G12C} behaves in a manner distinct from expectations based on historic studies of more commonly explored RAS mutants (Q61K, G12V, G12D) suggests that general assumptions of mutant RAS properties should be directly explored across the spectrum of oncogenic RAS mutations. KRAS^{G12C} may not be the only mutant RAS protein whose behavior deviates from the classic view of oncogenic RAS as a constitutively and fully active protein.

ARS-853 takes advantage of the unexpected nucleotide cycling features of KRAS^{G12C} detailed above and represents the first direct KRAS inhibitor to achieve cellular potency in the range of a drug candidate. Further optimization will be required to generate compounds suitable for *in vivo* studies, but this work presents a significant step toward a direct KRAS inhibitor for the treatment of patients with the KRAS^{G12C} mutation, which comprises 20% of lung cancers.

METHODS

Cell Lines and Reagents

Human cancer cell lines were purchased from the ATCC or the Korean Cell Line Bank (HCC-1171) and maintained at 37°C in a humidified atmosphere at 5% CO₂ and grown in RPMI-1640 or DMEM growth media (Gibco) supplemented with 10% fetal bovine serum (Gibco), 50 units/mL penicillin, and 50 µg/mL streptomycin (Gibco). NCI-H358, NCI-H23, A549, and A375 cell line identities were confirmed using the CellCheck 16 (IDEXX Bioresearch), an SNP-based profile authentication service, before studies were conducted. Cell lines utilized within the embodied work were purchased from ATCC (August 2014) and were carried for no longer than 12 cell passages. Erlotinib, afatinib, and trametinib were purchased from LC Laboratories. Recombinant human EGF was purchased from Life Technologies. All antibodies were purchased from Cell Signaling Technologies, except as follows: KRAS-specific antibody (clone C-19), NRAS-specific antibody (clone C-20), and HRAS-specific antibody (clone C-20) were from Santa Cruz Biotechnology; RAS-specific antibody (clone EPR3255) was from Abcam; and CRAF-specific antibody was from BD Biosciences.

Protein Expression and Purification

KRAS^{G12C}, WT, and G13C proteins were expressed in *E. coli* as truncated (1–169), hexahistidine-tagged forms as described by Ostrem and colleagues (6). For crystallography studies, the KRAS^{G12C} protein was expressed in *E. coli* and purified as described, including removal of the hexahistidine tag (6). Proteins used in biochemical studies were expressed and purified as described (6), except that the TEV cleavage (hexahistidine tag removal) and ion exchange chromatography steps were omitted. The resulting proteins were >95% pure as judged by SDS-PAGE. For SOS nucleotide exchange, the catalytic domain (594–1049) of SOS1 was expressed in *E. coli* and purified as described (6).

Crystallization, Data Collection, and Refinement

For X-ray crystallography, KRAS 1–169 (C51S/C80L/C118S) was used and the protein was prepared as described previously (6). Magnesium chloride (1 mmol/L final) and GDP (40 µmol/L final) were added to the freshly purified protein. After high-speed centrifugation, hanging drop crystallization conditions were set up by mixing 1:1 protein and reservoir solution (2.2 mol/L 3:2 NaH₂PO₄/K₂HPO₄, 0.2 mol/L Li₂SO₄, 0.1 mol/L glycine pH = 10.5). After several days at 20°C, thin plates were observed. The crystals were cryoprotected in the crystallization solution

supplemented with 20% glycerol, flash-frozen, and stored in liquid nitrogen prior to obtaining diffraction data at beamline 5.0.1. (100 K nitrogen stream, wavelength = 0.9774 Å) at the Berkeley Lab Advanced Light Source. Data were initially processed with iMosfilm, solved by molecular replacement using Phaser and refined to the indicated statistics using Refmac (29). The refined model showed no Ramachandran outliers, and 98.5% of the residues were in the favored region (30).

KRAS Biochemical Modification Assay

GDP-loaded, hexahistidine-tagged, truncated (1-169) KRAS proteins (G12C, WT, G13D, as indicated) at 2 μmol/L final concentration were incubated with the test compounds at the doses and time points indicated in a buffer containing 20 mmol/L HEPES pH 7.5, 150 mmol/L NaCl, 1 mmol/L MgCl₂, and 1 mmol/L DTT. Reactions were quenched by adding formic acid to 0.2%. The extent of covalent modification was determined by liquid chromatography, electrospray mass spectrometry analysis of the intact proteins on either a time of flight (TOF; Agilent 6530) or Q-Exactive (Thermo) mass spectrometer.

Nucleotide Exchange Assays

KRAS^{G12C} protein (truncated, hexahistidine tagged) was loaded with the indicated nucleotide (GDP or mantGDP) as described (6). For the exchange assays with incoming mant-nucleotide, 12 μL of the prepared protein (1.25 μmol/L) in reaction buffer containing 1 μmol/L of the indicated incoming nucleotide (mantGDP and mantGTP) was added to wells of a low-volume black-bottom plate. For studies with mant-nucleotide-loaded protein, 12 μL of the prepared protein (1.25 μmol/L) in reaction buffer containing 1 mmol/L of the indicated incoming nucleotide (GDP or GTP) was added to the plate. Exchange reactions were initiated by the addition of 3 μL of SOS (10 μmol/L), or 3 μL of EDTA (20 μmol/L), or buffer control as indicated, and the fluorescence was monitored for 45 minutes at 60-second intervals as described (6).

G12C Cell Engagement Assay

Cells (35 × 10³) adhered overnight were treated with compound at the indicated concentration and incubation time. After treatment, cells were washed twice with PBS buffer, and proteins were extracted using a buffer containing 9 mol/L urea, 10 mmol/L DTT, and 50 mmol/L ammonium bicarbonate, pH 8. Following iodoacetamide alkylation and trypsin digestion, the samples were analyzed by targeted LC/MS-MS analysis on a Dionex RSLCnano LC (Thermo Scientific) coupled with a Q-Exactive quadrupole orbitrap mass spectrometer (Thermo Scientific). Detailed descriptions of the sample processing and LC/MS-MS methods can be found in Supplementary Methods and Supplementary Table S6.

Modeling of Cellular Engagement Dose–Time Course Data

Cellular engagement time courses at multiple concentrations of ARS-853 in H358 cells were fit to the model shown in Fig. 3C using Kintek Explorer Pro software (31). Modeling parameter details are described in Supplementary Methods.

Heavy Isotopic Protein Standard Production and Nucleotide Loading

Heavy isotopic PSAQ protein standards (KRAS^{G12C} and WT-NRAS) were produced in an auxotrophic *E. coli* strain grown in ¹³C¹⁵N-lysine and ¹³C¹⁵N-arginine minimal media at Promise Advanced Proteomics (Grenoble). Proteins were purified as described above for biochemical studies. The heavy protein standards were subsequently loaded with 5'-Guanylyl imidodiphosphate (GMPPNP), a non-hydrolyzable GTP analogue, by sequential dilution and concentration with a centrifugal concentrator. Loading efficiency for KRAS^{G12C} was determined using a GDP-selective covalent RAS inhibitor in the biochemical engagement assay. High probe concentrations were used to ensure complete

covalent reaction with the heavy protein standard. Loading efficiency was determined to be 52%.

Active RAS Determination by RBD Pulldown Assay

Cells (2 × 10⁶) preattached to a 10-cm dish (or 1 × 10⁶ preattached to 6-well plate per well) were treated with the indicated concentrations of compound for the time indicated. RAS activity was determined by the RAS activation kit from Cell Signaling Technology according to the manufacturer's instructions. In brief, cells were lysed with 1 mL (or 0.5 mL) of lysis buffer containing 80 μg/mL of GST-tagged RBD for 10 minutes on ice. Cells were scraped off and lysate was centrifuged at 14,000 rpm for 5 minutes at 4°C. Pre-cleared lysates were subsequently added to pre-washed glutathione agarose beads for 1 hour at 4°C under constant rocking. The beads were subsequently pelleted and washed 3 times and eluted for Western blotting with 40 μL of 1× SDS-PAGE sample buffer. Immunodetection of RAS proteins was carried out with the following antibodies: KRAS (C-terminal specific) antibody (C-19; Santa Cruz Biotechnology; 1:250), NRAS (C-20; Santa Cruz Biotechnology; 1:250), HRAS (C-20; Santa Cruz Biotechnology; 1:250), and pan-RAS antibody (EPR3255; Abcam; 1:4,000).

RBD-MS Assay

Samples were prepared as described for the RAS-GTP pulldown assay by Western blotting above with the following modifications. Immediately before cell lysis, 50 ng each of heavy isotopic labeled, GMPPNP-loaded KRAS^{G12C} and WT-NRAS protein standards were added to the lysis buffer. After lysis, 10% of the cell lysate was removed for precapture MS analysis, and the remaining 90% was precipitated with glutathione beads. The captured material was eluted with MS elution buffer (0.1% SDS, 10 mmol/L DTT). Both the RBD eluted samples and precapture lysate samples were acetone precipitated, resuspended in a buffer containing 9 mol/L urea, 10 mmol/L DTT, and 50 mmol/L ammonium bicarbonate, pH 8, and subjected to trypsin digest and MS analysis as described above for the G12C cell engagement assay. A detailed description of the calculations used to determine the RAS-GTP fraction can be found in Supplementary Methods.

Lentivirus Generation and shRNA Constructs

For mutant KRAS overexpression, codon-optimized cDNAs encoding N-terminal FLAG-tagged human KRAS (G12V and G12C) were cloned into pLenti6.2/V5-DEST gateway vector or the T-REX Gateway vector pLenti6.3/TO/V5-DEST (LifeTech). For inducible ectopic expression of KRAS or LacZ for rescue experiments, NCI-H358 cells were stably transduced with the tetracycline repressor-based backbone vector pLenti3.3/TR from the ViraPower HiPerform T-REX Gateway vector kit as recommended by the manufacturer's instructions (referred to as T-REX⁺ NCI-H358 cells) and were utilized for both signaling and proliferation assay in Figs. 3D and 4A. MISSION shRNA TRC1.5 vector clones in the pLKO.1-puro backbone for KRAS and Luciferase were purchased from Sigma. The clone IDs for shRNAs are as follows: shKRAS #1 (TRCN0000033260), shKRAS #2 (TRCN0000033262), and shLuciferase (SHC007). Lentiviral particles were packaged in HEK293FT cells using the ViraPower Lentiviral expression system (LifeTech) and transduced at a multiplicity of infection of 5 using standard recommended procedures. Cell cultures were spinfected in the presence of 5 to 8 μg/mL polybrene and centrifuged at 600 ×g for 30 minutes at 37°C. Following spinfection cultures were replenished with fresh media.

3-D Agar-Based Colony Formation Assay

Cells (10,000–20,000) were seeded in 0.35% soft agar (SeaPlaque GTG agarose; Lonza) cultures (1 mL of 0.8% base, 1 mL of 0.35% cell layer, 1 mL of liquid top layer in 6-well plates). Cells were allowed to rest overnight in 3-D before treatment with compound. For compound treatment, DMSO or ARS-853 was supplied into the top liquid media layer. For shRNA experiments conducted in Fig. 3F, cells were seeded 48 hours after

transduction with indicated lentiviruses in media containing 1 $\mu\text{g}/\text{mL}$ puromycin either in 2-D or 3-D agar-based formats. After 12 to 14 days, colonies were stained with 0.05% crystal violet, and foci formation was scored with colony counting software (NIH ImageJ, particle analyzer).

Cell Proliferation Assays

For experiments conducted in 2-D adherent formats or 3-D ultra-low adherent formats, cells (800–1,200 per well) were seeded in standard tissue culture–treated 96-well format plates (Corning Costar #3903) or ultra-low attachment surface 96-well format plates (Corning Costar #3474). The day after plating, cells were treated with serial dilutions of indicated inhibitors. Five days later, cellular viability was assessed using CellTiter-glo (Promega) according to the manufacturer's instructions. IC_{50} calculations were performed in GraphPad Prism Version 6.0. For shRNA experiments conducted in Fig. 3F, cells (20,000) for the 2-D format were seeded into tissue culture–treated 6-well plates following lentiviral transduction as described above.

Proximity Ligation Assay

Protocols and reagents for the proximity ligation assay were based on the DuoLink *In Situ* Staining Kit (Sigma, DUO92014). Cells were allowed to adhere overnight onto 18-well microslides ibiTreated (Ibidi, #81826) in a humidity slide chamber. Following compound treatment, cells were washed with PBS and fixed with 3.7% paraformaldehyde for 15 minutes at 37°C in a humidity slide chamber. Cells were permeabilized (0.1% triton X-100) for 30 minutes at room temperature and stained with anti-KRAS antibody (clone C-19; Santa Cruz Biotechnology, 1:50) and anti-CRAF (BD Biosciences, 1:50) overnight at 4°C in a humidity slide chamber. Following a 3 \times wash, secondary DuoLink PLUS and MINUS PLA probes (Sigma, DUO92002 and DUO92004) were added for 2 hours at 37°C. Following three washes, a ligation and amplification reaction was performed following the manufacturer's instructions. In brief, the oligonucleotide-conjugated secondary antibodies were ligated together with a ligation reaction of 45 minutes at 37°C, and a rolling circle PCR amplification reaction for 100 minutes at 37°C (GFP version). Slides were subsequently air-dried for 1 hour at room temperature and mounted with ProLong Gold antifade (LifeTech) media with DAPI. The slides were imaged using a 40 \times objective on a FLOID XL fluorescent microscope (LifeTech). KRAS–CRAF interactions were quantified using DuoLink *In Situ* Image Tool software (Sigma) from merged TIFF color images of both the PLA signal and nuclei channel (DAPI stain). A minimum of 200 cells were quantified from three independent replicate wells for each treatment condition.

Cysteine Selectivity Profiling

NCI-H358 cells (1×10^6) were seeded overnight in 6-well plates and treated with compound for 4 hours at the indicated concentration. Cells were trypsinized and washed with PBS buffer. Cells were resuspended in a buffer containing 25 mmol/L Tris–HCl, pH 7.5, 150 mmol/L NaCl, 1% NP-40, 5% glycerol and protease inhibitor. Following probe sonication, cell extracts were treated with 100 $\mu\text{mol}/\text{L}$ iodoacetamide desthiobiotin for 1 hour at room temperature to label surface-exposed cysteines. After probe labeling, proteins were acetone precipitated and resuspended in a buffer containing 9 mol/L urea, 10 mmol/L DTT and 50 mmol/L ammonium bicarbonate, pH 8, processed, and digested with trypsin as described for the G12C cell engagement assay. The eluate from the Zeba desalting plates was diluted 1:1 with 100 mL of 25 mmol/L Tris–HCl pH 7.4, 150 mmol/L NaCl, and 0.1% NP-40, and the desthiobiotinylated peptides were enriched using high-capacity Streptavidin agarose beads (30 μL per sample, Thermo #20359). The beads were incubated with the sample for 1 hour and washed sequentially with 25 mmol/L Tris–HCl pH 7.4, 150 mmol/L NaCl, 0.1% NP-40; PBS; and water. Enriched peptides were eluted with 150 μL of 50% acetonitrile and 0.1% TFA, dried using a Savant SPD100 centrifugal evaporator (Thermo Scientific), and stored

at -20°C until LC/MS-MS analysis. A detailed description of the LC/MS-MS analysis procedure can be found in Supplementary Methods.

NIH-3T3 KRAS Transformation

3T3 cells (2×10^4) transduced with indicated mutant KRAS lentiviruses were selected for 1 week with 1 $\mu\text{g}/\text{mL}$ blastocidin and were subsequently plated in a top layer of 0.35% soft agar (SeaPlaque GTG agar; Lonza), cultured, and treated as described.

Cell-Cycle Analysis by Flow Cytometry

Cells plated in 6-well plates were treated for 72 hours as indicated. One hour prior to harvest, 2 $\mu\text{mol}/\text{L}$ 5-ethynyl-2'-deoxyuridine (EdU) was added to cultures to assess cycling cells. Cells were subsequently trypsinized, collected (including unattached cells), and washed with PBS. Cells were then fixed with 4% paraformaldehyde, permeabilized with saponin-based solution, and stained for EdU incorporation using the Click-iT EdU flow cytometry assay kit (LifeTech C10632) using the Alexa Fluor 488 azide per the provided instructions. DNA content was monitored by the addition of FxCycle Violet stain (LifeTech) 20 minutes prior to acquisition. Cell-cycle analysis was performed with a Miltenyi MACSQuant flow cytometer, and indicated populations were quantified using FlowJo software, V10.

Chemical Synthesis of Compounds

See supplementary information and Supplementary Fig. S12A–B.

Disclosure of Potential Conflicts of Interest

M.P. Patricelli reports receiving commercial research support from Janssen Biotech, Inc. and has ownership interest (including patents) in Wellspring Biosciences LLC. M.R. Janes has ownership interest (including patents) in Wellspring Biosciences LLC. L.-S. Li reports receiving commercial research support from Janssen Biotech, Inc. and has ownership interest (including patents) in Wellspring Biosciences LLC. U. Peters reports receiving commercial research support from Janssen Biotech, Inc. and has ownership interest (including patents) in Wellspring Biosciences LLC. J.M. Kucharski reports receiving commercial research support from Janssen Biotech, Inc. and has ownership interest (including patents) in Wellspring Biosciences LLC. T. Ely reports receiving commercial research support from Janssen Biotech, Inc. and has ownership interest (including patents) in Wellspring Biosciences LLC. S.J. Firdaus reports receiving commercial research support from Janssen Biotech, Inc. and has ownership interest (including patents) in Wellspring Biosciences LLC. A. Babbar reports receiving commercial research support from Janssen Biotech, Inc. and has ownership interest (including patents) in Wellspring Biosciences LLC. P. Ren has ownership interest (including patents) in Wellspring Biosciences LLC and is a consultant/advisory board member for the same. Y. Liu has ownership interest (including patents) in Wellspring Biosciences LLC and is a consultant/advisory board member for the same. No potential conflicts of interest were disclosed by the other authors.

Authors' Contributions

Conception and design: M.P. Patricelli, M.R. Janes, U. Peters, Y. Liu
Development of methodology: M.P. Patricelli, M.R. Janes, R. Hansen, L.V. Kessler, J.H. Chen

Acquisition of data (provided animals, acquired and managed patients, provided facilities, etc.): R. Hansen, U. Peters, L.V. Kessler, J.M. Kucharski, T. Ely, S.J. Firdaus, A. Babbar

Analysis and interpretation of data (e.g., statistical analysis, biostatistics, computational analysis): M.P. Patricelli, M.R. Janes, R. Hansen, U. Peters, J.M. Kucharski, J.H. Chen, A. Babbar, Y. Liu

Writing, review, and/or revision of the manuscript: M.P. Patricelli, M.R. Janes, J. Feng, T. Ely, P. Ren, Y. Liu

Administrative, technical, or material support (i.e., reporting or organizing data, constructing databases): L.-S. Li, L.V. Kessler, J.M. Kucharski, J. Feng

Study supervision: M.P. Patricelli, M.R. Janes

Other (designed and synthesized the molecules disclosed in this article): L.-S. Li

Other (designed and executed experiments): Y. Chen

Other (designed the molecules): P. Ren

Acknowledgments

The authors are grateful to Kevan Shokat for providing Compounds 11 and 12, discussion of the data, and comments on the manuscript, and to Frank McCormick for discussion. They acknowledge Shanghai Langtze Biomedical Technology for chemistry support on this program.

Atomic coordinates and structure factors for the ARS-853 crystal structure have been deposited to the Protein Data Bank (PDB: 5F2E).

Grant Support

This research is financially supported by Janssen Biotech, Inc. under a collaboration between Wellspring Biosciences LLC and Janssen Biotech.

The costs of publication of this article were defrayed in part by the payment of page charges. This article must therefore be hereby marked *advertisement* in accordance with 18 U.S.C. Section 1734 solely to indicate this fact.

Received September 10, 2015; revised January 4, 2016; accepted January 5, 2016; published OnlineFirst January 6, 2016.

REFERENCES

- Cox AD, Fesik SW, Kimmelman AC, Luo J, Der CJ. Drugging the undruggable RAS: mission possible? *Nat Rev Drug Discov* 2014;13:828–51.
- Sun Q, Burke JP, Phan J, Burns MC, Olejniczak ET, Waterson AG, et al. Discovery of small molecules that bind to K-Ras and inhibit Sos-mediated activation. *Angewandte Chemie* 2012;51:6140–3.
- Maurer T, Garrenton LS, Oh A, Pitts K, Anderson DJ, Skelton NJ, et al. Small-molecule ligands bind to a distinct pocket in Ras and inhibit SOS-mediated nucleotide exchange activity. *Proc Natl Acad Sci U S A* 2012;109:5299–304.
- Shima F, Yoshikawa Y, Matsumoto S, Kataoka T. Discovery of small-molecule Ras inhibitors that display antitumor activity by interfering with Ras.GTP-effector interaction. *Enzymes* 2013;34 Pt. B:1–23.
- Lim SM, Westover KD, Ficarro SB, Harrison RA, Choi HG, Pacold ME, et al. Therapeutic targeting of oncogenic K-Ras by a covalent catalytic site inhibitor. *Angewandte Chemie* 2014;53:199–204.
- Ostrem JM, Peters U, Sos ML, Wells JA, Shokat KM. K-Ras(G12C) inhibitors allosterically control GTP affinity and effector interactions. *Nature* 2013;503:548–51.
- Wang C, Weerapana E, Blewett MM, Cravatt BF. A chemoproteomic platform to quantitatively map targets of lipid-derived electrophiles. *Nat Methods* 2014;11:79–85.
- Singh A, Greninger P, Rhodes D, Koopman L, Violette S, Bardeesy N, et al. A gene expression signature associated with “K-Ras addiction” reveals regulators of EMT and tumor cell survival. *Cancer Cell* 2009;15:489–500.
- Collisson EA, Sadanandam A, Olson P, Gibb WJ, Truitt M, Gu S, et al. Subtypes of pancreatic ductal adenocarcinoma and their differing responses to therapy. *Nat Med* 2011;17:500–3.
- Foster R, Mudd C, Wiggins C, Torrance C. Abstract 4289: 3-Dimensional growth reveals KRAS dependency. *Cancer Res* 2013;73:4289.
- Fujita-Sato S, Galeas J, Truitt M, Pitt C, Urisman A, Bandyopadhyay S, et al. Enhanced MET translation and signaling sustains K-Ras driven proliferation under anchorage-independent growth conditions. *Cancer Res* 2015;75:2851–62.
- Vartanian S, Bentley C, Brauer MJ, Li L, Shirasawa S, Sasazuki T, et al. Identification of mutant K-Ras-dependent phenotypes using a panel of isogenic cell lines. *J Biol Chem* 2013;288:2403–13.
- Ahmadian MR, Zor T, Vogt D, Kabsch W, Selinger Z, Wittinghofer A, et al. Guanosine triphosphatase stimulation of oncogenic Ras mutants. *Proc Natl Acad Sci U S A* 1999;96:7065–70.
- Hunter JC, Manandhar A, Carrasco MA, Gurbani D, Gondi S, Westover KD. Biochemical and Structural Analysis of Common Cancer-Associated KRAS Mutations. *Mol Cancer Res* 2015;13:1325–35.
- Alessi DR, Saito Y, Campbell DG, Cohen P, Sihanandam G, Rapp U, et al. Identification of the sites in MAP kinase kinase-1 phosphorylated by p74raf-1. *EMBO J* 1994;13:1610–9.
- Dougherty MK, Muller J, Ritt DA, Zhou M, Zhou XZ, Copeland TD, et al. Regulation of Raf-1 by direct feedback phosphorylation. *Mol Cell* 2005;17:215–24.
- Pratilas CA, Taylor BS, Ye Q, Viale A, Sander C, Solit DB, et al. (V600E)BRAF is associated with disabled feedback inhibition of RAF-MEK signaling and elevated transcriptional output of the pathway. *Proc Natl Acad Sci U S A* 2009;106:4519–24.
- Sun C, Hobor S, Bertotti A, Zecchin D, Huang S, Galimi F, et al. Intrinsic resistance to MEK inhibition in KRAS mutant lung and colon cancer through transcriptional induction of ERBB3. *Cell Rep* 2014;7:86–93.
- Montero-Conde C, Ruiz-Llorente S, Dominguez JM, Knauf JA, Viale A, Sherman EJ, et al. Relief of feedback inhibition of HER3 transcription by RAF and MEK inhibitors attenuates their antitumor effects in BRAF-mutant thyroid carcinomas. *Cancer Discov* 2013;3:520–33.
- Molina-Arcas M, Hancock DC, Sheridan C, Kumar MS, Downward J. Coordinate direct input of both KRAS and IGF1 receptor to activation of PI3 kinase in KRAS-mutant lung cancer. *Cancer Discov* 2013;3:548–63.
- Trahey M, McCormick F. A cytoplasmic protein stimulates normal N-ras p21 GTPase, but does not affect oncogenic mutants. *Science* 1987;238:542–5.
- Ford B, Skowronek K, Boykevich S, Bar-Sagi D, Nassar N. Structure of the G60A mutant of Ras: implications for the dominant negative effect. *J Biol Chem* 2005;280:25697–705.
- Buss JE, Solski PA, Schaeffer JP, MacDonald MJ, Der CJ. Activation of the cellular proto-oncogene product p21Ras by addition of a myristylation signal. *Science* 1989;243:1600–3.
- Adari H, Lowy DR, Willumsen BM, Der CJ, McCormick F. Guanosine triphosphatase activating protein (GAP) interacts with the p21 ras effector binding domain. *Science* 1988;240:518–21.
- Young A, Lou D, McCormick F. Oncogenic and wild-type Ras play divergent roles in the regulation of mitogen-activated protein kinase signaling. *Cancer Discov* 2013;3:112–23.
- Evelyn CR, Biesiada J, Duan X, Tang H, Shang X, Papoian R, et al. Combined rational design and a high throughput screening platform for identifying chemical inhibitors of a Ras-activating enzyme. *J Biol Chem* 2015;290:12879–98.
- Patgiri A, Yadav KK, Arora PS, Bar-Sagi D. An orthosteric inhibitor of the Ras-Sos interaction. *Nat Chem Biol* 2011;7:585–7.
- Leshchiner ES, Parkhitko A, Bird GH, Luccarelli J, Bellairs JA, Escudero S, et al. Direct inhibition of oncogenic KRAS by hydrocarbon-stapled SOS1 helices. *Proc Natl Acad Sci U S A* 2015;112:1761–6.
- Winn MD, Ballard CC, Cowtan KD, Dodson EJ, Emsley P, Evans PR, et al. Overview of the CCP4 suite and current developments. *Acta Crystallogr D Biol Crystallogr* 2011;67:235–42.
- Chen VB, Arendall WB 3rd, Headd JJ, Keedy DA, Immormino RM, Kapral GJ, et al. MolProbity: all-atom structure validation for macromolecular crystallography. *Acta Crystallogr D Biol Crystallogr* 2010;66:12–21.
- Johnson KA. Fitting enzyme kinetic data with KinTek global kinetic explorer. *Methods Enzymol* 2009;467:601–26.

CANCER DISCOVERY

Selective Inhibition of Oncogenic KRAS Output with Small Molecules Targeting the Inactive State

Matthew P. Patricelli, Matthew R. Janes, Lian-Sheng Li, et al.

Cancer Discov 2016;6:316-329. Published OnlineFirst January 6, 2016.

Updated version Access the most recent version of this article at:
doi:[10.1158/2159-8290.CD-15-1105](https://doi.org/10.1158/2159-8290.CD-15-1105)

Supplementary Material Access the most recent supplemental material at:
<http://cancerdiscovery.aacrjournals.org/content/suppl/2016/01/06/2159-8290.CD-15-1105.DC1>

Cited articles This article cites 31 articles, 16 of which you can access for free at:
<http://cancerdiscovery.aacrjournals.org/content/6/3/316.full#ref-list-1>

Citing articles This article has been cited by 84 HighWire-hosted articles. Access the articles at:
<http://cancerdiscovery.aacrjournals.org/content/6/3/316.full#related-urls>

E-mail alerts [Sign up to receive free email-alerts](#) related to this article or journal.

Reprints and Subscriptions To order reprints of this article or to subscribe to the journal, contact the AACR Publications Department at pubs@aacr.org.

Permissions To request permission to re-use all or part of this article, use this link
<http://cancerdiscovery.aacrjournals.org/content/6/3/316>.
Click on "Request Permissions" which will take you to the Copyright Clearance Center's (CCC) Rightslink site.